

# We are IntechOpen, the world's leading publisher of Open Access books Built by scientists, for scientists

7,400

Open access books available

193,000

International authors and editors

210M

Downloads

Our authors are among the

154

Countries delivered to

TOP 1%

most cited scientists

14%

Contributors from top 500 universities



WEB OF SCIENCE™

Selection of our books indexed in the Book Citation Index  
in Web of Science™ Core Collection (BKCI)

Interested in publishing with us?  
Contact [book.department@intechopen.com](mailto:book.department@intechopen.com)

Numbers displayed above are based on latest data collected.  
For more information visit [www.intechopen.com](http://www.intechopen.com)



## Chapter

# Advanced Wideband Antenna Arrays for 5G Millimeter-Wave Spectrum at K- and Ka-Bands

*Mohammad Alibakhshikenari, Peiman Parand, Bal Virdee, Ignacio Garcia Zuazola, Sunil Kumar, Ali Zidour, Mohammad Soruri, Takfarinas Saber, Mohammad Naser-Moghadasi and Ernesto Limiti*

## Abstract

Millimeter-wave (mm-Wave) wireless communication systems play a central role in meeting the demands of next-generation wireless technologies such as 5G. This chapter presents the design and analysis of three advanced antenna arrays optimized for mm-Wave 5G wireless networks operating over K-band (18–27 GHz) and Ka-band (27–40 GHz). These structures feature radiation patches suspended above a common substrate, excited using three methods to achieve optimal performance. The first method utilizes a  $50\ \Omega$  open-ended microstrip-line balun to slot-line transition for effective energy coupling and excitation. The second method employs a  $50\ \Omega$ -microstrip feed network, ensuring consistent power distribution across array elements. Lastly, metallic-rods passing through the substrate provide direct excitation, facilitating robust mechanical and electrical integration. To address challenges, innovative techniques were implemented. Vertical metallic-vias suppress unwanted surface currents, while the spacing between radiating elements was optimized as multiples of half-wavelength to minimize interference and maximize array performance. Additionally, antenna elements were enclosed with metallic-walls to further enhance isolation and ensure predictable performance. Further strategies such as bowtie-like dipoles were incorporated to provide wider radiation apertures and better impedance matching. Power dividers were used to split input signals into multiple equal-phase outputs, boosting overall gain. Furthermore, the patches were embedded with slots to exhibit metasurface characteristics, enhancing bandwidth and radiation performance while maintaining compactness. The design methodologies and optimizations result in antenna arrays with superior performance metrics. The detailed analysis, innovative techniques, and demonstrated performance of the proposed antenna arrays establish them as strong candidates for practical deployment in advanced 5G mm-Wave networks and beyond.

**Keywords:** antenna array, millimeter-wave (mm-wave) spectrum, metallic-vias, open-ended microstrip-line balun, bowtie-like dipoles, slot-line transition, metallic-walls, power dividers, metasurface characteristics, 5G communications

## **1. Introduction**

The global rollout of 5G wireless communication systems is rapidly progressing, driven by the growing demand for faster, more reliable, and highly connected communication networks [1]. Unlike previous generations of cellular technology, 5G introduces transformative benefits, such as significantly faster internet speeds and the capacity to connect thousands of devices simultaneously [2–4]. These advancements facilitate revolutionary concepts like the Internet of Things (IoT) and the Internet of Everything (IoE), enabling the development of smart services capable of providing real-time information [5, 6]. These innovations are set to redefine industries, enhance automation, and create opportunities for intelligent and connected environments.

In the initial phase of deployment, 5G systems operate in frequency bands between 700 MHz and 3.8 GHz, which were traditionally used for earlier generations of mobile communication technologies. While these frequency bands provide foundational support for the network, the growing demand for bandwidth—driven by the increasing number of connected devices and rising data consumption—necessitates access to higher frequencies [7]. This demand has led to the exploration of the millimeter-wave (mm-Wave) spectrum, operating between 26 and 42 GHz, which offers significantly larger bandwidth and the potential to support high-capacity networks [8–10].

The mm-Wave spectrum, despite its potential, comes with significant challenges. Transmission in this band is affected by high propagation losses due to atmospheric absorption, free-space path loss, dielectric losses, radiation inefficiencies, and metallic losses in transmission lines [11]. To overcome these limitations, the focus of research has shifted to advanced antenna array technologies that can mitigate these losses while leveraging the wide bandwidth available in the mm-Wave spectrum [12].

The mm-Wave band has garnered widespread attention as a critical enabler for next-generation mobile communication standards beyond 5G [13]. Networks powered by mm-Wave technology are expected to deliver multi-gigabit data rates, exceptional capacity, and ultra-reliable mobile broadband speeds, extending even to suburban and rural areas. These capabilities will bridge the digital divide and support a wide array of applications, including telemedicine, autonomous transportation, smart cities, and more [14]. However, millimeter-wave signals have a limited ability to penetrate solid objects, such as buildings, making them suitable primarily for short-range applications in high-density environments like sports arenas, shopping malls, convention centers, and urban streetscapes where data congestion is prevalent [15].

The rising data traffic associated with modern applications exceeds the capabilities of current 5G systems operating at lower frequencies. This has necessitated a shift to mm-Wave frequencies, which provide access to much larger bandwidths capable of accommodating intense data demands [16]. The sub-20 GHz frequency bands are already heavily congested, leaving higher-frequency bands as the only viable solution. Prominent frequency ranges for 5G mm-Wave communication include 24–28, 37–40, and 64–71 GHz, which provide significant bandwidth for high-speed data transmission [17]. However, utilizing these bands introduces new challenges, including increased free-space path loss and hardware impairments [18, 19].

To address the challenges of path loss and attenuation in mm-Wave communications, high-gain beamforming antenna arrays with wide scanning angles are essential [20]. These arrays enhance beam coverage and improve the efficiency of signal propagation over mm-Wave channels. However, this improvement comes at a cost. Increasing

the number of antennas in an array to achieve higher gain also increases the complexity and cost of associated electronics, making mm-Wave antenna systems significantly more expensive than their counterparts operating at lower frequencies [21]. Beam-steering antenna arrays, integral components of massive multiple-input multiple-output (MIMO) systems, are indispensable for expanding system capacity and extending coverage in 5G networks [22]. These arrays provide the ability to steer signals in multiple directions simultaneously, enabling higher signal-to-noise ratios (SNR) and improved channel capacity without requiring additional spectrum resources [23].

Despite these advancements, designing compact and efficient antenna systems remains a significant challenge. The size of antennas is directly related to the operating wavelength [24], and reducing the spacing between adjacent radiating elements in antenna arrays is necessary to achieve compactness [25]. However, this reduction in spacing can lead to increased electromagnetic coupling between radiators, which negatively affects performance [26]. These effects include degradation of terminal impedance, reduced impedance bandwidth, and compromised radiation characteristics [27, 28]. This, in turn, impacts key performance metrics such as output signal-to-interference noise ratio, radiation efficiency, and radar cross-section [29, 30].

The primary challenge in designing mm-Wave and sub-terahertz antenna arrays lies in balancing the need for reduced physical size with the requirement to suppress mutual coupling between neighboring radiators while simultaneously enhancing radiation properties [31]. Achieving this balance requires innovative design approaches that address these competing demands. Recent research has explored several methods to mitigate mutual coupling and enhance array performance, such as optimizing element placement, introducing isolation structures, and leveraging novel materials and geometries. Our research team has investigated and reported various approaches to tackle these challenges, many of which will be discussed in this chapter to provide insights into the design and optimization of mm-Wave antenna arrays [2–4].

## **2. Millimeter-wave antennas for 5G communications systems**

In this section, a comprehensive study on the design process of millimeter-wave (mm-Wave) antennas with high-gain performances for 5G applications has been provided. Three published articles that operate over various 5G spectrums are discussed, and their capability for diverse applications, such as 5G mobile terminals, 5G cellular communications, and 5G on-demand wireless networks, is elaborated in depth [2–4]. Besides the operating working frequencies and radiation properties, interesting techniques have been applied to keep the dimensions of the antennas as small as possible and enhance the isolation between the radiation elements, which are the crucial factors for the proposed 5G applications. Such methods have been also described in detail.

### **2.1 Wideband endfire antenna array for 5G mm-wave mobile terminals**

According to the Third-Generation Partnership Project (3GPP) technical specification (TS 38.101-2 release 16.7.0), the 5G New Radio (NR) sub-millimeter-wave (sub-mm-Wave) spectrum allocations, classified as frequency range 2 (5G NR FR2), have been clearly defined to support the requirements of next-generation wireless communication [23]. Within this context, the broadband frequency ranges from 24.25 to 29.5 GHz, covering a span of 19.5%, and is identified as a key 5G mm-Wave band.

This frequency range is crucial for achieving the high data rates, low latency, and large capacity demanded by modern applications. Consequently, there is an urgent need for wideband antenna designs that not only provide high gain but also exhibit symmetric radiation patterns necessary for advanced beam scanning applications.

Meeting these design requirements poses significant challenges for both academic researchers and industry practitioners. Wideband antennas for 5G mm-Wave applications must simultaneously deliver excellent performance in terms of bandwidth, radiation efficiency, and beam scanning while adhering to stringent constraints on size, profile, and ground clearance. Compact, low-profile designs are particularly desirable for integration into mobile and compact devices. However, developing solutions that achieve these diverse and often competing objectives remains a highly complex task.

### 2.1.1 The proposed endfire antenna array

To address these challenges, a compact endfire antenna array is presented, operating in the frequency bands of 26, 28, and 30 GHz, which are essential for 5G NR mobile communications [2]. This design not only achieves superior performance but also overcomes some of the most pressing challenges in mm-Wave antenna engineering. The standout features of the proposed antenna array include:

1. *Compact and low-profile design:* The antenna array is highly compact, measuring only 19 mm in size, with an ultra-low profile of 0.712 mm and a ground clearance of just 1.9 mm. This makes the design ideal for space-constrained applications, including mobile devices and wearable technology.
2. *Wideband operation with high isolation:* The array effectively covers a wide frequency bandwidth, including lower bands such as the n258 band. Notably, it maintains an isolation level below 20 dB even with a 4.7 mm inter-element spacing. This performance is achieved without the need for additional decoupling structures, simplifying the design and reducing overall system complexity.
3. *Broad beam scanning capabilities:* The phased array enables a wide beam scanning range of  $\pm 68^\circ$  at 28 GHz, offering exceptional flexibility and adaptability for dynamic beamforming and steering applications.

### 2.1.2 Antenna element design

The design of the endfire antenna element was optimized for performance, compactness, and efficiency. As illustrated in **Figure 1**, the antenna employs a multilayer printed circuit board (PCB) configuration, with stacked substrates constructed from Rogers RO4350B (dielectric constant,  $\epsilon_r = 3.66$ ; loss tangent,  $\tan\delta = 0.0037$ ) and a prepreg bonding layer made from Rogers RO4450F ( $\epsilon_r = 3.52$ ;  $\tan\delta = 0.004$ ). This multilayer approach ensures both structural integrity and enhanced electrical performance.

The antenna's radiating elements consist of two bow tie-like dipoles, printed on the top (M1) and bottom (M3) layers of the PCB. These dipoles are connected to a truncated ground plane that serves as a reflector. The bowtie dipole topology has been specifically modified to minimize the overall size of the radiating structure, making it suitable for applications requiring small clearance.

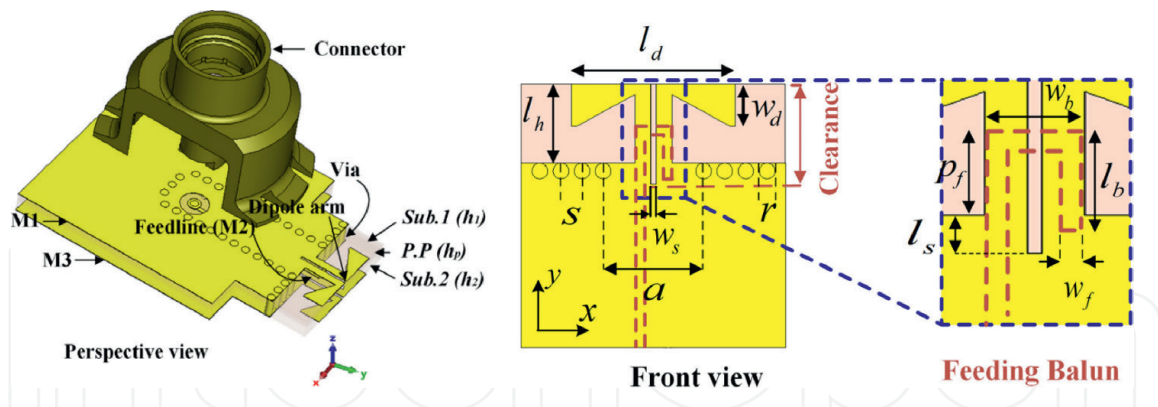


**Figure 1.**  
 Configuration of the antenna element [2].

The dipoles are excited *via* a feeding structure etched on the opposite side of the substrate. This feeding mechanism uses a 50  $\Omega$  open-end microstrip-line balun (M2) to slot-line transition. The slot-line transition provides efficient energy coupling to the dipoles, ensuring optimal excitation. The stacked substrates not only facilitate the integration of the feeding structure but also improve the bandwidth and radiation characteristics of the antenna.

One of the key challenges in this design is addressing the potential impedance mismatch and radiation efficiency degradation caused by coupling between the dipole and the bottom ground plane (M3). To mitigate this, a clearance is introduced below the dipole, effectively reducing coupling effects. Furthermore, a pair of dipoles is incorporated into both the top and bottom metallic layers (M1 and M3), which enhances impedance matching and improves endfire radiation characteristics.

Metallic vias are strategically introduced between the metallic layers as grounding pins. These vias play a crucial role in suppressing unwanted surface waves, thereby improving impedance bandwidth and overall radiation efficiency. The use of metallic vias also stabilizes the antenna's electrical performance by reducing parasitic effects, making the design robust and reliable for 5G applications.

The proposed endfire antenna array is compact and low-profile configuration making it highly suitable for integration into 5G mobile devices, small cells, and other compact systems. The wideband performance, coupled with excellent beam scanning capabilities, ensures that the antenna can support a diverse range of applications, from high-speed mobile communication to beamforming in dense urban environments. The elimination of additional decoupling structures further simplifies manufacturing and reduces costs, making the design both practical and scalable for widespread deployment.

### 2.1.3 Antenna array design

To achieve high gain and beamforming capabilities with a wide beam scanning range, the proposed antenna element was extended into a linear  $1 \times 4$  antenna array. This mm-Wave array design features a profile height of less than  $0.07\lambda$ , making it ultra-low-profile and suitable for compact applications. The spacing between adjacent elements was carefully set at 4.7 mm ( $0.44\lambda$  at 28 GHz), close to the half-wavelength requirement, to ensure adequate port isolation for efficient beam scanning.

The compact radiating aperture results in overall dimensions of just  $19 \times 1.9 \times 0.712 \text{ mm}^3$ , making it ideal for integration into 5G systems where space constraints are critical.

The feeding structure uses MMPX coaxial-type connectors, which are overlaid on the top ground plane. Each array element is excited by an open-end strip-line connected to the inner conductor of the connector through a metal *via*. Surface wave suppression vias were strategically placed around each feeding structure to reduce power loss in the strip-line, thereby improving the overall efficiency of the antenna array.

To validate and verify the proposed design methodology, an antenna array prototype was fabricated and subjected to comprehensive measurements. The S-parameters were evaluated using a Vector Network Analyzer (VNA) model: R&S ZVA40. Photographs of the fabricated prototype and the measurement setup are shown in **Figure 2(a)**. **Figure 2(b)** and **(c)** compare the simulated and measured reflection coefficients ( $S_{ii}$ ) and mutual coupling values ( $S_{ij}$ ) between the array elements. The measurements indicate that the array achieves a  $-10 \text{ dB}$  operating bandwidth spanning from 24 to 34 GHz, with mutual coupling values better than  $-15 \text{ dB}$ , ensuring minimal interference between elements. These results demonstrate excellent agreement between the simulated and measured data, validating the accuracy of the proposed design approach.

**Figure 2(d)** presents the 2D polar radiation patterns for one of the array elements (port 2) in both the ( $xoy$ ) plane (E-plane) and the ( $xoz$ ) plane (H-plane) at 24 GHz, 26 GHz, 28 GHz, and 30 GHz. The measured and simulated results show a strong correlation, particularly in the vertical plane, with stable and symmetric endfire radiation patterns across the operating frequency range. This symmetry ensures consistent performance for beamforming applications.

The realized gain of the antenna array in the  $+y$  direction across the operating frequencies is plotted in **Figure 2(e)**. Within the primary frequency band of interest, from 24.25 to 29.5 GHz, the antenna array achieves consistent endfire realized gains. The simulated gain values range from 7.93 to 8.66 dBi, while the measured values are slightly lower, varying between 7.56 and 8.14 dBi. These results highlight the efficiency of the design, as the measured and simulated gains are in close agreement. Moreover, the peak realized gains observed in the simulations are nearly identical to the endfire gains, indicating a minimal loss in the beamforming direction.

While the antenna array performs well within the intended frequency band, a drop in endfire gain is observed in simulations for frequencies above 30 GHz. This reduction in gain is attributed to increased impedance mismatch and radiation inefficiencies at higher frequencies, which is consistent with typical limitations in mm-Wave antenna designs. However, within the designated bands (24.25–29.5 GHz), the antenna array demonstrates stable performance, making it suitable for 5G applications.

The proposed mm-Wave  $1 \times 4$  antenna array offers an innovative solution for compact, high-performance beamforming in 5G communication systems. Its ultra-low-profile design, compact radiating aperture, and effective integration of surface wave suppression techniques enable wideband operation with excellent radiation and gain characteristics. The fabrication and testing results confirm the reliability and accuracy of the design, with measured parameters closely matching simulations. The stable and symmetric endfire radiation patterns, along with consistent realized gains across the operating band, make this antenna array a strong candidate for advanced mm-Wave applications requiring efficient and compact beam scanning solutions.

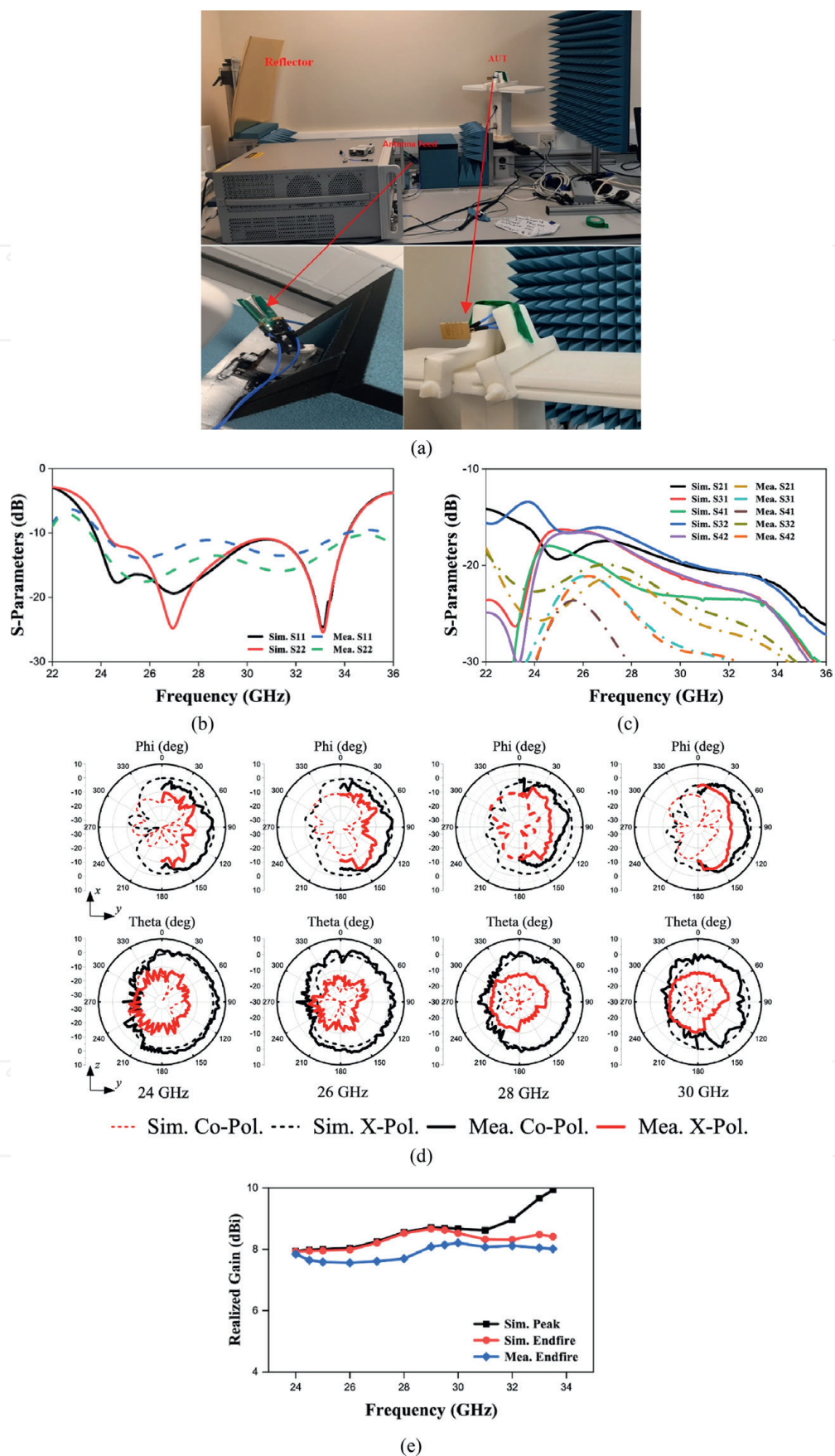


**Figure 2.** (a) Photographs of the fabricated antenna array and far-field measurement setup, (b) reflection coefficient response, (c) mutual coupling response, (d) radiation patterns of the array @ 24, 26, 28, and 30 GHz, and (e) realized gain response of the array in the endfire direction [2].



#### 2.1.4 State-of-the-art comparison

To evaluate the proposed design's performance, a comparison with other relevant mm-Wave endfire antenna arrays is presented, as summarized in **Table 1**. This section highlights how the proposed antenna array compares with its peers in terms of key performance metrics, including bandwidth, gain, compactness, and beam scanning range.

The proposed design achieves a bandwidth of 34%, which is comparable to [32] (37%) and [36] (27%) and significantly better than [35] (15%) and [37] (22%). While [34] achieves a higher bandwidth (42%), the proposed design's bandwidth is well-suited for accommodating the entire 5G NR band (24.25–29.5 GHz), which is a critical requirement for modern 5G systems. Additionally, the proposed design maintains excellent performance without requiring additional structural complexity.

In terms of realized gain, the proposed design achieves values ranging from 7.5 to 8.1 dBi. This gain is slightly lower than the higher ranges observed in Ref. [32] (9.1–13.8 dBi), [33] (10–12 dBi), and [36] ( $\geq 12$  dBi). However, it is comparable to [34] (8 dBi) and [37] (6.6–8.1 dBi). While the gain is somewhat limited, it meets the minimum acceptable levels set by 3GPP regulations and remains practical for 5G applications where compactness is prioritized.

The proposed design achieves a beam scanning range of  $\pm 68^\circ$ , which is broader than [37] ( $\pm 54^\circ$ ) and comparable to Ref. [36] ( $\pm 70^\circ$ ). However, Refs. [33, 34] achieve wider scanning ranges of  $\pm 75^\circ$  and  $\pm 90^\circ$ , respectively. The proposed design balances a good scanning range with structural simplicity and compactness, whereas some designs with larger scanning ranges may require additional complexities or larger inter-element spacing.

The compactness of the proposed design is one of its standout features. With an element width of  $0.29\lambda$ , a profile of  $0.07\lambda$ , and a clearance of  $0.18\lambda$ , it is smaller than most other designs, such as Ref. [32] ( $0.16\lambda$  profile and  $0.82\lambda$  clearance), [34] ( $0.08\lambda$  profile and  $0.73\lambda$  clearance), and [35] ( $0.07\lambda$  profile and  $0.23\lambda$  clearance). Only Ref. [33] achieves a lower profile ( $0.02\lambda$ ) and clearance ( $0.51\lambda$ ) but at the cost of a larger element width of  $0.55\lambda$ , which affects overall compactness. The proposed design's low profile and small clearance make it particularly well-suited for integration into compact mobile devices.

The proposed design features an inter-element spacing of 4.7 mm ( $0.44\lambda$  at 28 GHz) and achieves good isolation without requiring additional decoupling structures. This contrasts with some other designs, such as Refs. [32, 34], which rely on more complex methods to manage mutual coupling. This simplicity makes the proposed design more practical for manufacturing and integration.

The proposed antenna array effectively balances bandwidth, gain, beam scanning range, and compactness, making it highly competitive with existing designs. While it does not achieve the highest gain or scanning range, its exceptional compactness, low profile, and small clearance make it particularly suitable for integration into modern mobile devices. Furthermore, its ability to maintain good isolation without requiring additional decoupling structures ensures both simplicity and cost-effectiveness, positioning it as a practical and high-performing solution for 5G NR mm-Wave applications.

## 2.2 Design of high gain base station antenna array with wide bandwidth for mm-wave cellular communication systems

In recent years, significant research has focused on developing antennas for 5G wireless systems operating in the 37–40 GHz frequency band [6, 13–17]. However,

Ref.	Antenna Type	Array Number	Operating Band (GHz)	BW (%)	Array Gain (dBi)	Scanning (degree)	Element Width ( $\lambda$ )	Profile ( $\lambda$ )	Clearance ( $\lambda$ )
[32]	SIW-fed Metasurface	1 × 4	26.6-38.7	37	9.1-13.8	—	0.16	0.16	0.82
[33]	Dipole	1 × 8	26.5-38.0	36	10-12	±75	0.55	0.02	0.51
[34]	Quasi-Yagi	1 × 4	26-40	42	8	±90	0.55	0.08	0.73
[35]	Quasi-Yagi	1 × 4	25.9-30.2	15	9.0-9.6	—	0.30	0.07	0.23
[36]	Dipole	1 × 8	25-33	27	≥12	±70	0.36	0.15	0.13
[37]	Quasi-Yagi	1 × 4	24-30	22	6.6-8.1	±54	0.32	0.12	0
<b>Authors' Work in [2]</b>	<b>Bow-Tie Dipole</b>	<b>1 × 4</b>	<b>24-34</b>	<b>34</b>	<b>7.5-8.1</b>	<b>±68</b>	<b>0.29</b>	<b>0.07</b>	<b>0.18</b>

**Table 1.**  
 Comparison with other relevant endfire mm-Wave antenna arrays [2].

many of these designs cannot be directly adopted for base station applications due to their insufficient gain, which is critical for achieving the required coverage and signal quality in mm-Wave base station deployments.

A novel antenna array suitable for 5G mm-Wave base station applications was investigated and practically tested in Ref. [3]. The design addresses the limitations of previous works by employing a  $2 \times 2$  array configuration for each radiating structure within the antenna array. This approach significantly enhances the overall gain, making the array well-suited for the demanding requirements of mm-Wave base stations.

### 2.2.1 Single antenna element design

The single element antenna that forms the foundation of the 5G mm-Wave array here is shown in **Figure 3**. The geometry resembles a two-pronged fork, with excitation provided through a microstrip feedline edge-connected to the U-shaped arm of the fork [19, 25]. This unconventional configuration was selected for its superior impedance matching characteristics compared to a standard rectangular patch antenna. Enhanced impedance matching ensures minimal power loss at the feed point, which is critical for high-frequency operations like mm-Wave communication.

While the quasi-fork-like antenna configuration offers improved impedance matching, it does have a smaller effective aperture compared to a conventional rectangular patch antenna operating at the same center frequency. This limitation results in a slightly lower gain for a single element. Despite this, the configuration's simplicity, improved matching, and suitability for integration into compact arrays make it a practical choice for base station designs.

The single antenna element is constructed on a Rogers 5880 dielectric substrate, known for its excellent electrical properties, which make it ideal for high-frequency applications such as mm-Wave communication. The substrate has a relative permittivity of 2.2, a thickness of 0.254 mm, and a low loss tangent of 0.0009, minimizing dielectric losses and ensuring efficient radiation performance. The overall dimensions of the antenna element are  $10 \times 6 \text{ mm}^2$ , which balances compactness with acceptable performance metrics.

### 2.2.2 Antenna array design

To enhance the performance and scalability of the proposed antenna design, it was implemented into a series of progressively larger antenna arrays, starting with

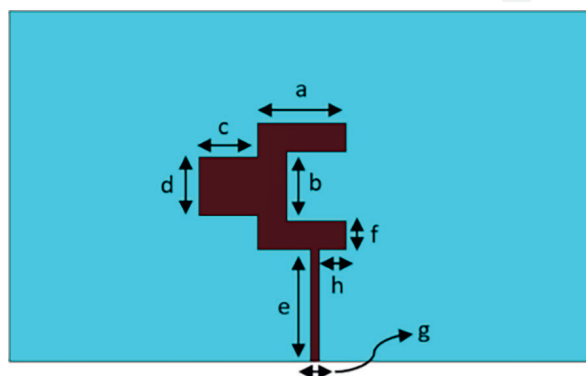


**Figure 3.** Geometry of the proposed single antenna element [3].

an  $8 \times 8$  array and extending to  $8 \times 16$  and  $8 \times 32$  arrays. Each iteration of the design maintains careful attention to factors such as spacing, feedline design, and impedance matching to optimize performance for mm-Wave applications.

#### 2.2.2.1 $8 \times 8$ antenna array

The first stage of the array design utilizes 16 individual antennas arranged in an  $8 \times 8$  configuration, as shown in **Figure 4(a)**. These antennas are interconnected using power dividers and excited through a  $50\text{-}\Omega$  feed network. Several key design considerations were applied to ensure optimal performance:

- The spacing between the radiating elements was set as a multiple of  $0.5\lambda$ . This minimizes mutual coupling effects, which can degrade array performance by introducing interference between adjacent elements. The precise spacing was optimized through simulation and analysis to achieve the best radiation characteristics.
- The feedline lengths were calculated to ensure phase coherency and power parity at all individual antennas. This ensures uniform excitation of all elements, which is critical for maintaining the gain and beamforming capabilities of the array. Without this optimization, the array would suffer from uneven radiation patterns and reduced efficiency.
- The compact design results in an overall array size of  $25.5 \times 27.5 \text{ mm}^2$ , making it suitable for applications where space is at a premium.

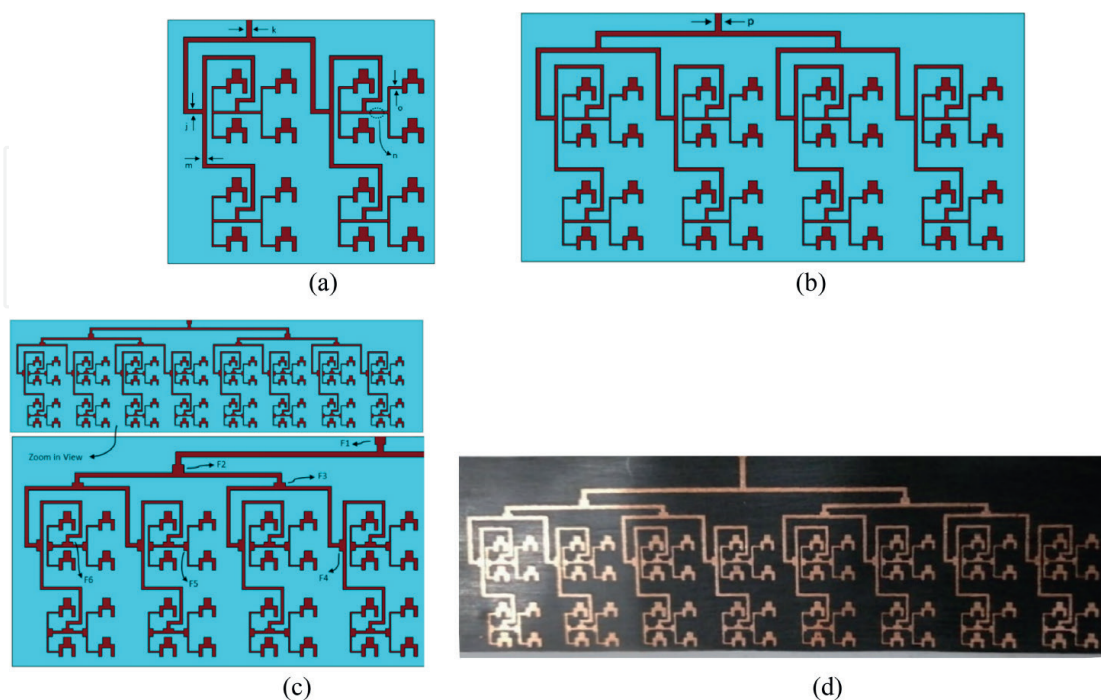


**Figure 4.** Geometry of the antenna array (a)  $8 \times 8$  array, (b)  $8 \times 16$  array, (c) simulated layout of  $8 \times 32$  array, and (d) fabricated prototype [3].

#### 2.2.2.2 $8 \times 16$ antenna array

To further boost gain and improve coverage, the  $8 \times 8$  array was expanded into an  $8 \times 16$  configuration, consisting of 32 antenna elements, as illustrated in **Figure 4(b)**. This was achieved by combining two  $8 \times 8$  arrays using a power divider. Key enhancements include:

- A power divider splits the input signal into two equal-phase output signals, which are then applied to each of the two  $8 \times 8$  arrays. This approach ensures consistent performance across the entire 32-element array.
- A quarter-wave transformer is integrated with the power divider to ensure impedance matching at the input. Proper matching minimizes signal reflection and maximizes power transfer to the array elements.
- Like the  $8 \times 8$  array, the feedlines are designed to maintain phase coherency and power equity across all elements of the array. This is critical for achieving uniform radiation and preventing degradation of the array's gain and radiation characteristics.
- The overall size of the  $8 \times 16$  array is  $27.5 \times 55 \text{ mm}^2$ . Despite the increased number of elements, the design maintains a relatively compact form factor.

#### 2.2.2.3 $8 \times 32$ antenna array

Building on the success of the  $8 \times 16$  design, the array was further scaled to an  $8 \times 32$  configuration, consisting of 64 antenna elements, as shown in **Figure 4(c)**. This design maintains the same foundational principles of power division, impedance matching, and feedline optimization:

- The  $8 \times 32$  array was constructed by combining two  $8 \times 16$  arrays using additional power dividers. This modular approach ensures scalability while preserving phase coherency and power balance.
- As with the  $8 \times 16$  array, a quarter-wave transformer is used with the power divider to maintain impedance matching. This ensures efficient signal distribution across all 64 elements.
- Despite the large number of elements, the array achieves a compact overall size of  $30 \times 110 \text{ mm}^2$ . This makes it suitable for use in base stations or other high-performance mm-Wave communication systems.

#### 2.2.2.4 Key design considerations across arrays

1. The element spacing (a multiple of  $0.5\lambda$ ) effectively reduces mutual coupling, which can otherwise lead to performance degradation in terms of gain and radiation patterns.
2. By ensuring phase coherency and power parity across all elements, the design achieves consistent radiation characteristics and prevents erosion of gain, which is critical in beamforming applications.

3. The modular approach to extending the array ensures that performance enhancements, such as increased gain and broader beam coverage, can be achieved without introducing significant complexity.
4. Each configuration maintains a balance between high performance and a compact form factor, ensuring suitability for mm-Wave applications, such as 5G base stations.

#### 2.2.2.5 Simulated and measured performance of the antenna arrays

The simulated and measured performance of the proposed antenna design, including the single element and its array configurations ( $8 \times 8$ ,  $8 \times 16$ , and  $8 \times 32$ ), demonstrates its suitability for 5G mm-Wave applications. The reflection coefficients for each configuration are shown in **Figure 5**, with the single element resonating at 38.5 GHz, the  $8 \times 8$  array at 39.0 GHz, the  $8 \times 16$  array at 39.1 GHz, and the  $8 \times 32$  array at 37.2 GHz. The measured results are in close agreement with the simulations, validating the design accuracy.

The radiation patterns for the single antenna element and the arrays in the  $\phi = 0^\circ$  and  $\phi = 90^\circ$  planes are displayed in **Figures 5(c)** and **(d)**. The single antenna element achieves a gain of 7.6 dBi, which is adequate for mobile handset applications but insufficient for 5G base stations that must overcome significant signal attenuation due to path loss, multipath effects, and atmospheric absorption. Its radiation beam is wide,

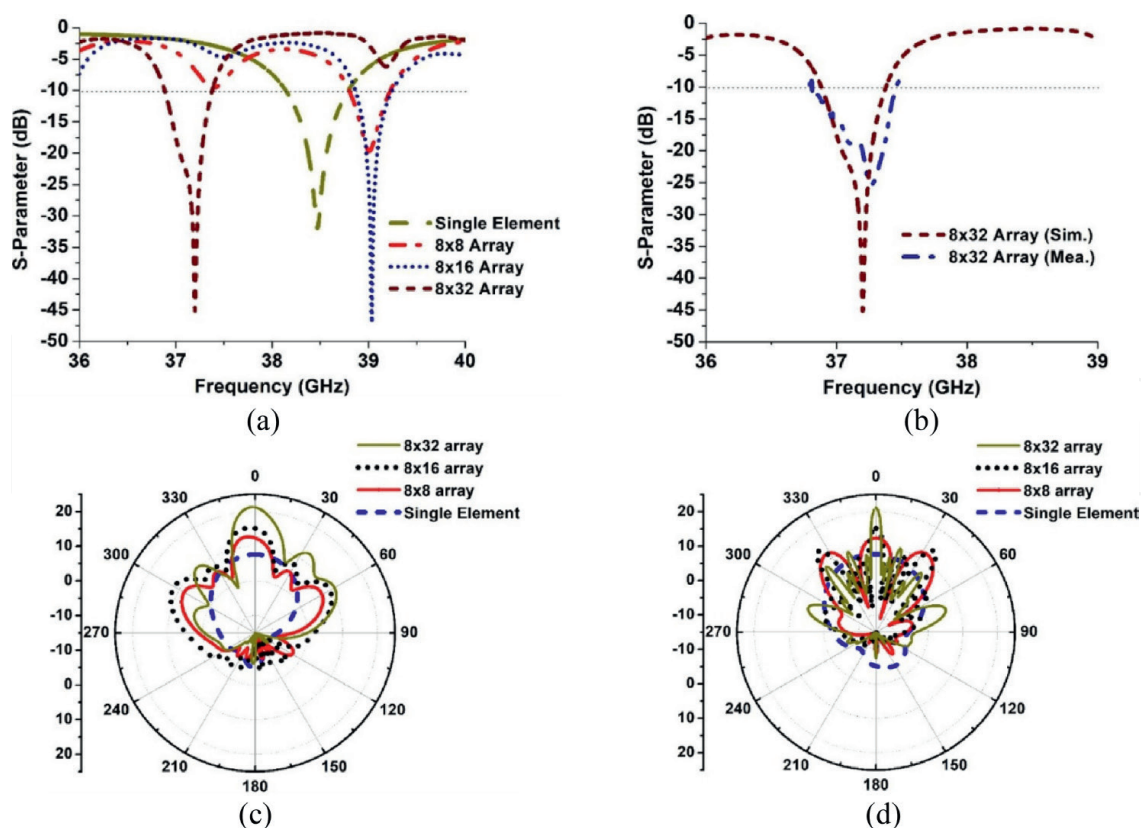


**Figure 5.** (a) Simulated reflection coefficient response of the single element and the antenna arrays, that is,  $8 \times 8$ ,  $8 \times 16$ ,  $8 \times 32$ , and (b) simulated and measured reflection coefficient responses of the  $8 \times 32$  array. Polar radiation patterns of the single antenna element and the three arrays ( $8 \times 8$ ,  $8 \times 16$ , and  $8 \times 32$ ), (c)  $\phi = 0^\circ$  plane radiation pattern, and (d)  $\phi = 90^\circ$  plane radiation pattern [3].

with an angular width of  $82.5^\circ$  in the  $\varphi = 90^\circ$  plane, making it less directed and less suitable for base station applications.

The  $8 \times 8$  array improves the gain to 13 dBi, but the side lobes in the  $\varphi = 0^\circ$  plane are suppressed to less than  $-6$  dB, while in the  $\varphi = 90^\circ$  plane they are suppressed to less than  $-3$  dB. These higher side lobe levels can lead to interference, limiting its effectiveness. The array narrows the angular width to  $18.4^\circ$ , providing a more focused beam compared to the single element.

The  $8 \times 16$  array further enhances the gain to 15.3 dBi, which is acceptable for base station use. However, the side lobes remain a concern, with suppression to less than  $-6$  dB in the  $\varphi = 0^\circ$  plane and less than  $-4$  dB in the  $\varphi = 90^\circ$  plane. The angular width narrows to  $7.2^\circ$  in the  $\varphi = 90^\circ$  plane, offering improved directivity compared to the smaller arrays.

The  $8 \times 32$  array achieves a substantial gain of 21.2 dBi, meeting the high-gain requirements of 5G mm-Wave base stations. It also demonstrates significant improvement in side lobe suppression, with side lobes reduced to less than  $-10$  dB in the  $\varphi = 0^\circ$  plane and less than  $-12$  dB in the  $\varphi = 90^\circ$  plane, making it suitable for practical applications. The beam becomes highly directed, with an angular width of just  $4.1^\circ$  in the  $\varphi = 90^\circ$  plane, ensuring efficient energy concentration and minimal interference.

This study verifies the feasibility of the proposed antenna design for large array configurations, particularly for 5G mm-Wave base stations. The results highlight the progressive improvement in gain and beam focusing as the array size increases. However, further work is needed to optimize the side lobe levels, especially for the smaller arrays, and to develop dual-polarized configurations to enhance the array's performance for advanced 5G applications.

### 2.3 State-of-the-art comparison

Over the years, significant advancements have been made in mm-Wave antenna array designs for 5G communication systems. **Table 2** compares the proposed  $8 \times 32$  antenna array with several recently reported designs, focusing on parameters such as the number of elements, center frequency, gain, substrate permittivity, and dimensions. The analysis highlights the advantages of the proposed design in terms of compactness and performance while noting areas for potential improvement.

The proposed  $8 \times 32$  array achieves a gain of 21.2 dBi at 37.2 GHz, which is competitive with several state-of-the-art designs. For instance, the  $8 \times 8$  array in Refs. [46, 47] achieves gains of 22 dBi at 39 and 28 GHz, respectively, using a stacked multilayer PCB structure and independent control of phase and amplitude at each radiating element. However, the proposed design is more compact, with dimensions of  $110 \times 30$  mm<sup>2</sup> compared to the  $100 \times 90$  mm<sup>2</sup> and  $100.6 \times 96.2$  mm<sup>2</sup> of these arrays.

The  $8 \times 32$  array in Ref. [48] demonstrates a higher gain of 25.7 dBi at 35 GHz but comes with a much larger form factor ( $212 \times 56$  mm<sup>2</sup>), approximately 3.6 times the size of the proposed design. While Ref. [48] achieves better gain, its significantly larger size limits its suitability for compact applications, where the proposed design offers a more practical solution.

The compact dimensions of the proposed antenna array ( $110 \times 30$  mm<sup>2</sup>) are a standout feature, making it significantly smaller than most comparable designs. For example: (1) The dual-band  $4 \times 3$  MIMO array in Ref. [38] has a gain of 13 dBi at 38 GHz but has much larger dimensions of  $122 \times 156$  mm<sup>2</sup>, (2) The  $8 \times 8$  metallic array in Ref. [45] achieves a high gain of 24 dBi at 26 GHz but lacks detailed size specifications, and metallic structures are generally bulkier, and (3) The aperture-coupled

Refs.	No. of elements	Center freq. (GHz)	Gain (dBi)	Substrate permittivity ( $\epsilon_r$ )	Dimensions (mm)
[38]	4 × 3	28	12.6	2.2	122 × 156
[38]	4 × 3	38	13	2.2	122 × 156
[39]	1 × 4	26.87	~5–6	3.35	5 × 5
[39]	1 × 4	38.5	~5–6	3.35	5 × 5
[40]	1 × 2	26.87	~5–6	3.35	5 × 5
[41]	2 × 2	37	12.8	2.2	20 × 8
[42]	2 × 2	29	14	2.2	9.7 × 9.7
[43]	4 × 4	30.1	11.35	2.94	90 × 54
[44]	1 × 8	33.5	14.1	2.2	58 × 5.5
[12]	1 × 8	36	16.9	2.2	50 × 40
[45]	8 × 8	26	24	—	—
[46]	8 × 8	39	22	3.3	100 × 90
[47]	8 × 8	28	22	2.55	100.6 × 96.2
[48]	8 × 32	35	25.7	2.22	212 × 56
<b>Authors' Work in [3]</b>	<b>8 × 32</b>	<b>37.2</b>	<b>21.2</b>	<b>2.2</b>	<b>110 × 30</b>

**Table 2.**  
 Comparison of the proposed antenna array with recent works [3].

patch array in Ref. [43] operates at 30.1 GHz with a gain of 11.35 dBi but occupies a large area of 90 × 54 mm<sup>2</sup>. The proposed design's compact form factor makes it highly suitable for applications requiring high performance in limited space, such as 5G base stations or other mm-Wave systems in urban or dense environments.

The proposed array demonstrates excellent beamwidth and side lobe suppression. Its angular width of 4.1° and side lobe levels of less than –10 dB (in the  $\varphi = 0^\circ$  plane) and less than –12 dB (in the  $\varphi = 90^\circ$  plane) represents a substantial improvement in performance. By contrast: (1) The 8 × 8 array in Refs. [46, 47] achieves good gain but does not explicitly address side lobe suppression, a critical factor for reducing interference; and (2) The array in Ref. [48] offers high gain but with limited information on beamwidth and side lobe levels, which are crucial for practical deployment in 5G systems.

The proposed design uses a substrate with a permittivity of 2.2, which is commonly used in high-frequency designs due to its low dielectric loss and high efficiency. Other works, such as Refs. [38, 41, 42], also employ substrates with similar permittivity, demonstrating a standard approach for minimizing loss in mm-Wave designs. However, designs such as Refs. [43, 46] use substrates with higher permittivity (e.g.,  $\epsilon_r = 2.94$  and 3.3), which can increase the dielectric loss but may help reduce size in specific configurations.

When considering overall performance, the proposed design strikes a balance between gain, compactness, and practical features such as side lobe suppression. While designs like Ref. [48] achieve higher gain, their significantly larger size limits their practicality in compact applications. Similarly, while smaller arrays such as Refs. [38, 41, 43] are compact, they deliver lower gains and do not match the beamwidth or side lobe suppression of the proposed design.



The proposed  $8 \times 32$  antenna array offers a strong balance between gain, compact size, and side lobe suppression. With a gain of 21.2 dBi, an angular width of  $4.1^\circ$ , and superior side lobe performance, it is well-suited for 5G mm-Wave applications. Compared to other designs, it stands out for its compactness, achieving high performance in a much smaller form factor. While higher gain designs exist, such as Ref. [48], their larger size makes them less practical for applications requiring compact integration. This balance of features positions the proposed array as a competitive and versatile solution in the state-of-the-art mm-Wave antenna landscape.

## 2.4 Broadband 3-D shared aperture high isolation nine-element antenna array for on-demand millimeter-wave 5G applications

A novel 3D shared aperture  $3 \times 3$  antenna array design, introduced in Ref. [4], is proposed for millimeter-wave (mm-Wave) 5G applications operating in the 24–28.4 GHz frequency range. The array employs hexagonal-shaped patches elevated above a common substrate and excited *via* metallic rods passing through the substrate. A key feature of this design is the inclusion of isolation walls that decouple individual antennas, effectively reducing mutual coupling and preserving far-field performance. To enhance gain and radiation efficiency, the patches are engineered with metasurface characteristics by incorporating hexagonal-shaped concentric slots of decreasing diameters. This innovative design enables the array to serve both single-aperture and shared aperture applications by utilizing subarrays to cover specific portions of the bandwidth for different time- or frequency-shared applications.

### 2.4.1 3D shared aperture nine-element antenna array

The geometry of the proposed 3D shared aperture nine-element antenna array is illustrated in **Figure 6(a)**. The array features hexagonal-shaped patches constructed on a base dielectric substrate made of Rogers RT5880, a material selected for its low loss tangent ( $\tan\delta = 0.0009$ ) and relative permittivity ( $\epsilon_r = 2.2$ ), which ensure high efficiency at mm-Wave frequencies. The dielectric substrate has a thickness of 0.2 mm and is supported by a metallic ground plane of 0.8 mm thickness.

The radiating patches are elevated 3.35 mm above the dielectric substrate using metallic rods with a diameter of 0.4 mm. These rods serve a dual purpose: they physically support the patches and function as the excitation mechanism by connecting to the feed network. The rods protrude through the base substrate and are insulated from the ground plane metallization layer, ensuring that unwanted interactions with the ground plane do not degrade antenna performance. Elevating the patches effectively reduces surface current interactions between adjacent antennas, which could otherwise lead to performance degradation. The overall size of the basic  $3 \times 3$  antenna array is compact, measuring  $20 \times 20 \times 3.35 \text{ mm}^3$ .

Mutual coupling between closely spaced radiating elements in an antenna array can distort radiation patterns and degrade overall far-field performance. To address this challenge, isolation walls are introduced around each individual antenna, as shown in **Figure 6(b)**. These walls, made from a perfect electric conductor, effectively suppress near-field radiation emanating from adjacent antennas. This technique ensures high isolation without altering the compact size of the array, maintaining the integrity of its physical footprint while preserving performance.

To further improve the performance of the antenna array, each hexagonal patch is loaded with concentric hexagonal slot rings of decreasing diameters, as depicted

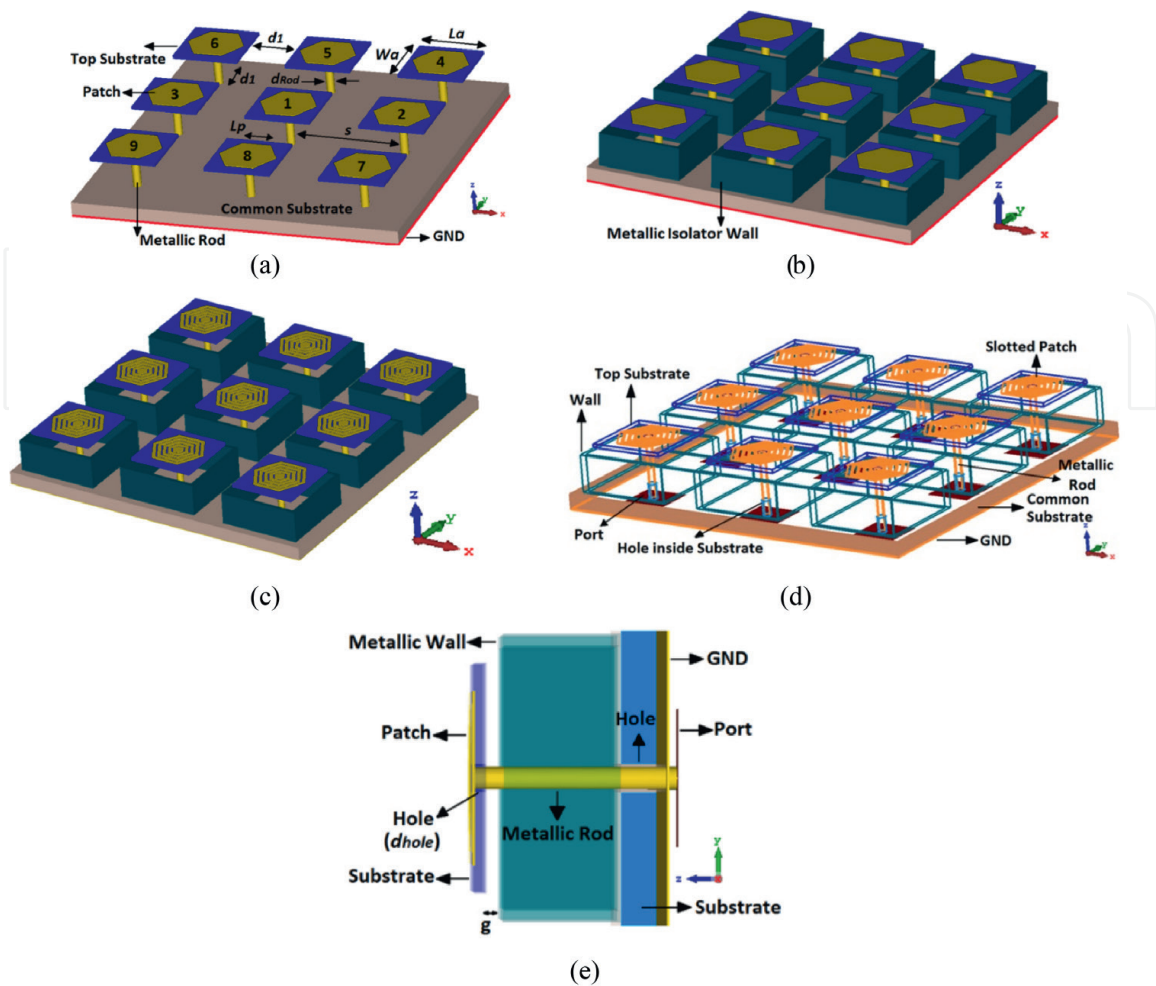


**Figure 6.** 3-D shared aperture nine-element  $3 \times 3$  array antennas, (a) basic array, (b) antenna array with the isolation walls, (c) array antennas with isolation walls and loaded with metasurface slots, (d) the array's schematic-view, and (e) the single element's side-view [4].

in **Figure 6(c)–(e)**. These slots are of subwavelength circumference, and each slot has a width of 0.08 mm. When exposed to electromagnetic (EM) waves, the slot-loaded patches behave as metasurfaces, as described in Refs. [14–16]. Metasurfaces are engineered surfaces with unique electromagnetic properties that enhance the effective aperture of the antenna, resulting in improved gain and radiation efficiency.

The integration of metasurface characteristics magnifies the aperture of the antenna array without increasing its physical dimensions. This technique leverages the interaction between EM waves and the subwavelength slots, enabling the array to deliver high performance across a broad bandwidth.

#### 2.4.2 Performance improvements with isolation walls and metasurface slots

The results obtained from 3D electromagnetic solvers, namely computer systems technology (CST) Microwave Studio and Ansoft high frequency simulation software (HFSS), as shown in **Figure 7**, demonstrate the significant performance enhancements achieved by incorporating isolation walls and metasurface slots into the antenna array. Notably, these improvements are realized without increasing the physical size of the array, maintaining its compact form factor.

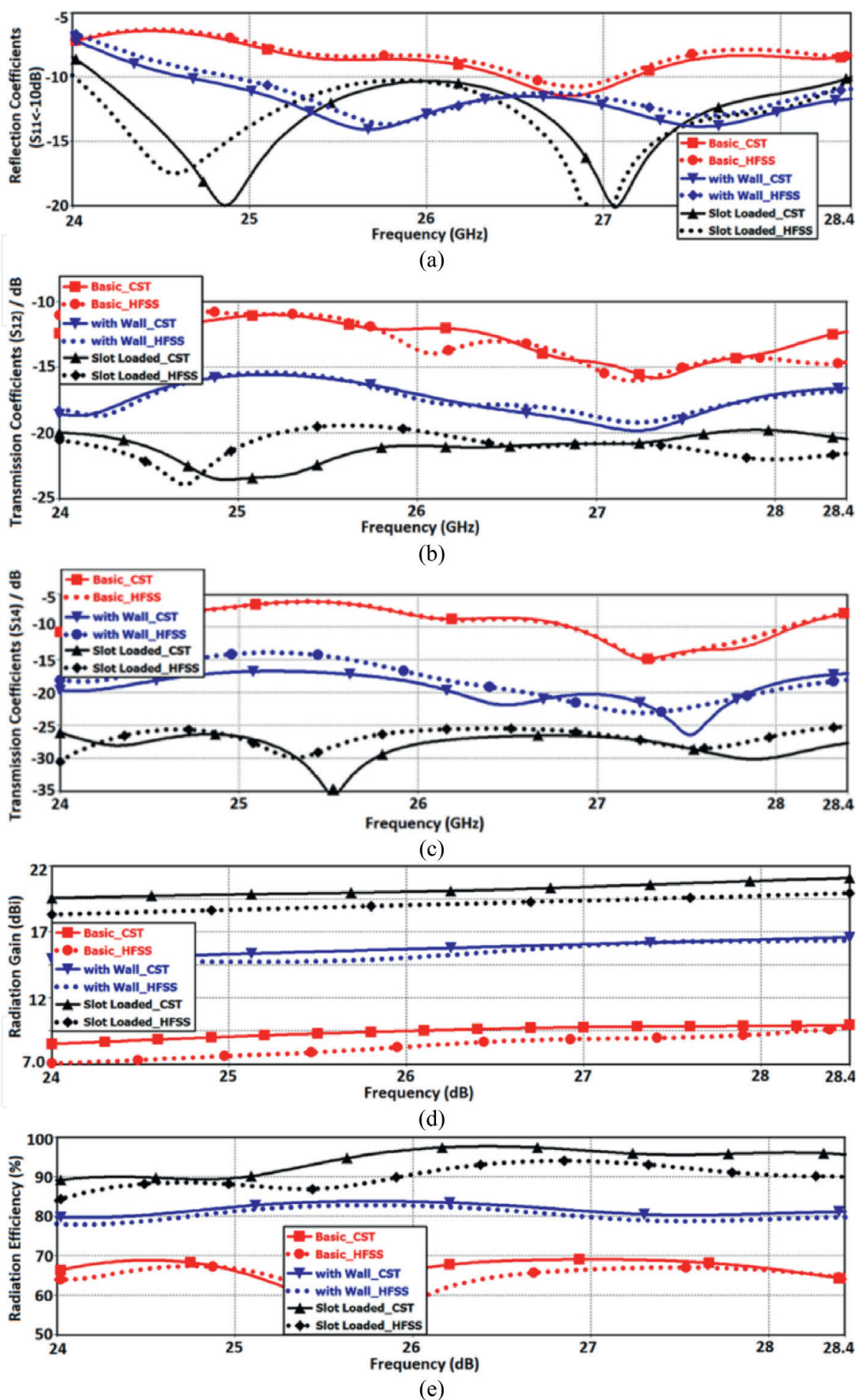


Figure 7.  $S$ -parameter response of the proposed antenna array, (a) reflection coefficient ( $S_{11}$ ), (b) transmission-coefficient between antennas #1 & #2 ( $S_{12}$ ), (c) transmission-coefficient between antennas #1 & #4 ( $S_{14}$ ), (d) radiation gain, and (e) radiation efficiency [4].

The introduction of isolation walls and metasurface slots substantially increases the array's impedance bandwidth. As shown in **Figure 7(a)**, the bandwidth of the final structure is extended by 4.4 GHz compared to the basic array design. This represents a sixfold increase in bandwidth, making the array suitable for broader operational frequencies within the mm-Wave 5G spectrum. The ability to achieve such a substantial improvement without increasing the physical dimensions of the antenna highlights the effectiveness of these design modifications.

**Figures 7(b)** and **(c)** illustrate the enhanced isolation between radiating elements in the array due to the incorporation of isolation walls. The symmetric nature of the design allows for the isolation performance to be assessed between representative pairs of elements, such as elements 1 & 2 and elements 1 & 4. The results indicate an isolation improvement of more than 10 dB in both cases compared to the basic model. This significant reduction in mutual coupling ensures better far-field performance and minimizes interference, which is critical for multi-element arrays used in 5G applications.

In addition to the improvements in bandwidth and isolation, the gain and radiation efficiency of the array are also significantly enhanced. **Figures 7(d)** and **(e)** show that the gain of the array increases by an average of 10.5 dBi compared to the basic design. Similarly, radiation efficiency is improved by 25%, which is a notable enhancement for an array operating in the challenging mm-Wave spectrum. These improvements ensure better signal strength and reduced power losses, making the array more effective for practical 5G applications.

The integration of isolation walls and metasurface slots into the  $3 \times 3$  antenna array design results in significant performance enhancements across key metrics, including bandwidth, isolation, gain, and efficiency. These improvements are achieved without compromising the array's compact size, demonstrating the effectiveness of these design modifications. The significant gains in bandwidth (a sixfold increase), isolation (10 dB improvement), and radiation efficiency (25% enhancement) position this array as a highly capable and practical solution for on-demand mm-Wave 5G applications.

#### *2.4.3 State-of-the-art comparison*

A comparative analysis of the proposed  $3 \times 3$  antenna array with previously published designs operating within the same frequency band is presented in **Table 3**. The parameters considered for comparison include array dimensions, substrate properties, bandwidth, maximum gain, and maximum efficiency. This analysis highlights the advantages of the proposed design in terms of gain and efficiency while maintaining a compact footprint, making it a viable solution for mm-Wave applications such as 5G wireless communications.

The proposed antenna array has a compact size of  $20 \times 20 \text{ mm}^2$ , which is significantly smaller than the arrays in Ref. [50] ( $99.2 \times 17.45 \text{ mm}^2$ , [53] ( $130 \times 90 \text{ mm}^2$ ). The only comparable designs in terms of size are those in Refs. [49, 51], which also feature compact footprints of  $20 \times 20 \text{ mm}^2$  and  $27 \times 25 \text{ mm}^2$ , respectively. Despite its small size, the proposed design achieves superior performance in terms of gain and efficiency compared to these designs.

The proposed design utilizes a 0.8 mm Rogers RT5880 substrate, which has excellent electrical properties, including a low loss tangent ( $\tan\delta = 0.0009$ ) and a relative permittivity ( $\epsilon_r = 2.2$ ), making it ideal for high-frequency applications. Other designs, such as Refs. [49, 51], use Rogers substrates (RO4350B and RO4003C) with slightly

Ref.	Size (mm <sup>2</sup> )	Substrate	Bandwidth/freq. Range (GHz)	Max. gain (dBi)	Max. eff. (%)
[49]	20 × 20	Two different layers: (i) 1 mm FR4 (ii) 0.254 mm Rogers RO4350B	5.25/24.25–29.5	10	85
[50]	99.2 × 17.45	0.254 mm Rogers RO5880	6.78/24.35–31.13	19.88	86
[51]	27 × 25	0.508 mm Rogers RO4003C	5/24–29	9	—
[52]	130 × 90	0.508 mm Rogers RO4003C	3/28–31	9.6	—
<b>Authors' Work in [4]</b>	<b>20 × 20</b>	<b>0.8 mm Rogers RO5880</b>	<b>4.4/24.0–28.4</b>	<b>21</b>	<b>98</b>

**Table 3.**

The proposed antenna array is compared with other arrays reported in the literature [4].

different thicknesses and properties, but they do not achieve the same level of performance as the proposed design.

The bandwidth of the proposed array is 4.4 GHz (24.0–28.4 GHz), which is slightly narrower than that of [49] (5.25 GHz) and [50] (6.78 GHz) but still adequate for most mm-Wave 5G applications. The designs in Refs. [51, 52] have bandwidths of 5 GHz and 3 GHz, respectively, which are narrower than [50] and comparable to the proposed design.

The proposed array achieves a maximum gain of 21 dBi, which is significantly higher than the gains of other designs, including Refs. [49] (10 dBi), [51] (9 dBi), and [52] (9.6 dBi). The closest competitor in terms of gain is Ref. [50], which achieves a gain of 19.88 dBi. However, Ref. [50] has a much larger footprint (99.2 × 17.45 mm<sup>2</sup>), making the proposed design superior for applications requiring compact form factors.

The proposed design demonstrates a maximum efficiency of 98%, surpassing the reported efficiencies of other designs. For instance, Refs. [49, 50] achieve efficiencies of 85% and 86%, respectively. The efficiency of Refs. [51, 52] is not reported, but their relatively lower gain suggests that their efficiency is likely inferior to that of the proposed array.

### 3. Conclusion

This chapter presented a comprehensive design and analysis of three innovative antenna arrays optimized for wideband operation in 5G millimeter-wave spectra. Various advanced techniques have been proposed and implemented to enhance key performance metrics such as frequency bandwidth, isolation, and radiation properties, all while maintaining compact physical dimensions. These techniques include the use of isolation walls, metasurface-inspired slots, and carefully optimized feeding mechanisms, which collectively improve array performance without adding complexity to the overall structure. The simplicity of the feeding mechanisms also ensures the practicality and feasibility of the designs for real-world implementations.

The antenna arrays presented here exhibit several notable advantages, including compact dimensions, wide operational bandwidth, high gain, and excellent efficiency.

Additionally, the arrays demonstrate stable and acceptable radiation patterns, low profiles, and cost-effectiveness, making them ideal candidates for 5G millimeter-wave wireless networks. The straightforward manufacturing process further enhances their appeal for large-scale production, ensuring scalability and reliability for widespread deployment.

Through a detailed comparison with state-of-the-art designs, the antenna arrays described here are shown to achieve a superior balance of compactness, performance, and practicality. With significant bandwidth enhancements—up to six times greater than baseline designs—alongside improvements in isolation (10 dB or more) and radiation efficiency (an increase of up to 25%), these arrays address the key challenges of mm-Wave communication. Notably, the integration of metasurface-inspired elements and isolation walls provides substantial performance gains without increasing the physical size, positioning these arrays at the forefront of compact high-performance antenna solutions.

The exceptional gain levels, such as 21 dBi for the  $8 \times 32$  array configuration, and efficiency up to 98%, surpass the performance of many comparable designs in the literature. Despite their superior performance, the proposed arrays maintain a compact form factor, which is critical for modern 5G applications where space constraints are a key concern. Furthermore, their ability to support shared aperture applications and subarray configurations allows for flexible use in time- or frequency-shared scenarios, catering to the diverse demands of dynamic 5G networks.

The cost-effective and straightforward manufacturing process, leveraging commercially available materials and simple design principles, ensures that these arrays are not only technically advanced but also economically viable. This balance of innovation, efficiency, and scalability makes the proposed antenna arrays strong candidates for widespread adoption in 5G millimeter-wave wireless networks and potentially beyond, in future communication systems.

By addressing the core challenges of mm-Wave antenna design—such as bandwidth, isolation, efficiency, and compactness—the work presented in this chapter provides a foundational approach for developing robust, high-performance solutions for next-generation communication technologies. The designs presented in this chapter exemplify the potential to bridge the gap between cutting-edge research and practical deployment, making a significant contribution to the evolution of wireless networks.

IntechOpen

### Author details

Mohammad Alibakhshikenari<sup>1\*</sup>, Peiman Parand<sup>1</sup>, Bal Virdee<sup>2</sup>,  
Ignacio Garcia Zuazola<sup>2</sup>, Sunil Kumar<sup>2</sup>, Ali Zidour<sup>3</sup>, Mohammad Soruri<sup>4</sup>,  
Takfarinas Saber<sup>5</sup>, Mohammad Naser-Moghadasi<sup>6</sup> and Ernesto Limiti<sup>1</sup>

1 Electronics Engineering Department, University of Rome “Tor Vergata”, Rome, Italy

2 Center for Communications Technology, London Metropolitan University, London,  
United Kingdom

3 Faculty of Technology, Department of Electrical Systems Engineering, University of  
M'hamed Bougara, Boumerdes, Algeria

4 Faculty of Ferdows Technical, University of Birjand, Birjand, Iran


5 Lero, Science Foundation Ireland Centre for Software, School of Computer Science,  
University of Galway, Galway, Ireland

6 Computer and Electrical Engineering Department, Science and Research Branch,  
Islamic Azad University, Tehran, Iran

\*Address all correspondence to: alibakhshikenari@ing.uniroma2.it

### IntechOpen

---

© 2025 The Author(s). Licensee IntechOpen. This chapter is distributed under the terms of the Creative Commons Attribution License (<http://creativecommons.org/licenses/by/4.0>), which permits unrestricted use, distribution, and reproduction in any medium, provided the original work is properly cited. 

## References

- [1] Mendonça S et al. The rise of 5G technologies and systems: A quantitative analysis of knowledge production. *Telecommunications Policy*. 2022;**46**(4):102327
- [2] Zidour A et al. Wideband endfire antenna Array for 5G mmWave mobile terminals. *IEEE Access*. 2024;**12**:39926-39935
- [3] Sehrai DA et al. Design of high gain base station antenna array for mm-wave cellular communication systems. *Scientific Reports*. 2023;**13**:4907
- [4] Alibakhshikenari M et al. Broadband 3-D shared aperture high isolation nine-element antenna Array for on-demand millimeter-wave 5G applications. *Optik*. 2022;**267**:169708
- [5] Rappaport TS, Xing Y, MacCartney GR, Molisch AF, Mellios E, Zhang J. Overview of millimeter wave communications for fifth-generation (5G) wireless networks—With a focus on propagation models. *IEEE Transactions on Antennas and Propagation*. 2017;**65**(12):6213-6230
- [6] Nguyen VL, Lin P, Hwang R. Enhancing misbehavior detection in 5G vehicle-to-vehicle communications. *IEEE Transactions on Vehicular Technology*. 2020;**69**(9):9417-9430
- [7] Storck CR, Duarte-Figueiredo F. A survey of 5G technology evolution, standards, and infrastructure associated with vehicle-to-everything communications by internet of vehicles. *IEEE Access*. 2020;**8**:117593-117614
- [8] Sharaf MH, Zaki AI, Hamad RK, Omar MMM. A novel dual-band (38/60 Ghz) patch antenna for 5G Mobile handsets. *Sensors*. 2020;**20**:2541
- [9] Peng M, Zhao A. High performance 5G millimeter-wave antenna array for 37-40 GHz mobile application. In: *International Workshop on Antenna Technology (iWAT)*. Nanjing, China: IEEE; 2018. pp. 1-4
- [10] Park J, Choi D, Hong W. 37-39 GHz vertically-polarized end-fire 5G antenna array featuring electrically small profile. In: *2018 IEEE International Symposium on Antennas and Propagation & USNC/URSI National Radio Science Meeting*, Boston, MA, USA, 08-13 July 2018. IEEE; 2018. pp. 637-638
- [11] Abbasi MAB, Abbasi QH. Development Challenges of Millimeter-Wave 5G Beamformers. In: Tafazolli R, Wang C-L, Chatzimisios P, editors. *Wiley 5G Ref*. Wiley; 2020. DOI: 10.1002/9781119471509.w5GRef226
- [12] Li A, Luk K-M. Millimeter-wave end-fire magneto-electric dipole antenna and arrays with asymmetrical substrate integrated coaxial line feed. *IEEE Open Journal of Antennas and Propagation*. 2021;**2**:62-71
- [13] Xiao M et al. Millimeter wave communications for future mobile networks. *IEEE Journal on Selected Areas in Communications*. 2017;**35**(9):1909-1935
- [14] Bang J, Chung H, Hong J, Seo H, Choi J, Kim S. Millimeter-wave communications: Recent developments and challenges of hardware and beam management algorithms. *IEEE Communications Magazine*. 2021;**59**(8):86-92
- [15] Ghafoor KZ et al. Millimeter-wave communication for internet of vehicles: Status, challenges, and perspectives.



IEEE Internet of Things Journal.  
2020;7(9):8525-8546

[16] Hong W et al. The role of millimeter-wave technologies in 5G/6G wireless communications. IEEE Journal of Microwaves. 2021;1(1):101-122

[17] Khan Z et al. Performance evaluation of 5G millimeter-wave-based vehicular communication for connected vehicles. IEEE Access. 2022;10:31031-31042

[18] Zakeri H et al. Path loss model estimation at indoor environment by using deep neural network and CatBoost for wireless application. IEEE Access. 2024;12:159070-159085

[19] Azizpour R et al. Multi-channel radio-over-fiber communication systems through modulation instability phenomenon. IEEE Photonics Journal. 2024;16(5):1-13

[20] Karim BA, Ali HK. A novel beamforming technique using mmWave antenna arrays for 5G wireless communication networks. Digital Signal Processing. 2023;134:103917

[21] Siddiqui SI et al. A dual-band high-gain beam steering antenna Array for 5G Sub-6 GHz Base station. Scientific Reports. 2024;14:26517

[22] El Mrini M, Mchbal A. Naima Amar Touhami, design of a 240 elements antenna system for 5G massive MIMO applications with an inclined beam and two operating modes. Journal of Electromagnetic Waves and Applications. 2024;38(16):1796-1810

[23] Wang Y, Xue Q, Hu Z, Liao S. Mixed-modes-enabled element-level beamforming antenna with enhanced isolation for phased array applications. IEEE Transactions on Antennas and Propagation. 2024;72(5):4577-4582

[24] Zandamela A et al. Digital pattern synthesis with a compact MIMO antenna of half-wavelength diameter. AEU - International Journal of Electronics and Communications. 2021;135:153728

[25] Pan W, Liu Y-H, Zhao Z-Q, Liu Q-H. Sparse antenna Array design methodologies: A review. Journal of Electronic Science and Technology. 2024;22(3):100276.3

[26] Abdalmalak KA, Yousfi AE, Vargas DS. Massive MIMO antenna arrays for low-frequency bands. In: Innovation in MIMO Systems [Working Title]. IntechOpen; 17 Dec 2024. DOI: 10.5772/intechopen.1007820

[27] Yousfi AE et al. Miniaturized dual-polarized, high-gain, and wideband dielectric resonator antenna for low band massive MIMO applications. Progress in Electromagnetics Research-PIER. 2024;179:101-111

[28] Yousfi AE, Atia Abdalmalak K, Lamkaddem A, Vargas DS. Miniaturized broadband dual-polarized dielectric resonator antenna using characteristic modes. In: 2023 17th European Conference on Antennas and Propagation (EuCAP), Florence, Italy, 26-31 March. IEEE; 2023. pp. 1-4

[29] Althuwayb AA et al. Design technique to mitigate unwanted coupling in densely packed radiating elements of an antenna array for electronic devices and wireless communication systems operating in the millimeter-wave band. AEU - International Journal of Electronics and Communications. 2023;159:154464

[30] Zheng Q, Wang J, PourMohammadi P, Pang X. Dual-band metasurface-based closely packed antennas by controlling surface wave propagation. IEEE Antennas

- and Wireless Propagation Letters. 2024;**23**(5):1633-1637
- [31] Ghosh S, Sen D. An inclusive survey on array antenna design for millimeter-wave communications. *IEEE Access*. 2019;**7**:83137-83161
- [32] Li T, Chen ZN. Wideband substrate-integrated waveguide-fed endfire metasurface antenna array. *IEEE Transactions on Antennas and Propagation*. 2018;**66**(12):7032-7040
- [33] Ta SX, Choo H, Park I. Broadband printed-dipole antenna and its arrays for 5G applications. *IEEE Antennas Wireless Propag. Lett*. 2017;**16**:2183-2186
- [34] Di Paola C, Zhang S, Zhao K, Ying Z, Bolin T, Pedersen GF. Wideband beam-switchable 28 GHz quasi-yagi array for mobile devices. *IEEE Transactions on Antennas and Propagation*. 2019;**67**(11):6870-6882
- [35] Hwang I-J et al. Quasi Yagi antenna array with modified folded dipole driver for mmWave 5G cellular devices. *IEEE Antennas and Wireless Propagation Letters*. 2019;**18**:971-975
- [36] Strytsin I, Zhang S, Pedersen GF, Morris AS. Compact quad mode planar phased array with wideband for 5G mobile terminals. *IEEE Transactions on Antennas and Propagation*. 2018;**66**(9):4648-4657
- [37] Liu Y, Zhao C, Yue Z, Ren A, Jia Y. A horizontally polarized endfire antenna with complete ground for 5GmmWave applications. *Microwave and Optical Technology Letters*. 2020;**62**(12):3936-3944
- [38] Elhabbash T, Skaik T. Design of dual-band dual-polarized MIMO antenna for mm-wave 5G base stations with octagonal prism structure. In: *IEEE 7th Palestinian International Conference on Electrical and Computer Engineering (PICECE)*. Gaza, Palestine: IEEE; 2019. pp. 1-6
- [39] Siddiqui Z et al. Dual-band dual-polarized antenna for mm-wave 5G base station antenna Array. In: *14th European Conference on Antennas and Propagation (EuCAP)*. Copenhagen, Denmark: IEEE; 2020. pp. 1-4
- [40] Siddiqui Z et al. Dual-polarized filtering antenna for mm-wave 5G base station antenna array. In: *15th European Conference on Antennas and Propagation (EuCAP)*, Dusseldorf, Germany, 22-26 March 2021. IEEE; 2021. pp. 1-4
- [41] Khan J et al. Design of a millimeter-wave MIMO antenna array for 5G communication terminals. *Sensors*. 2022;**22**:2768
- [42] Li K-X, Wu Y-W, Hao Z-C. A 5G millimeter-wave circularly polarized planar antenna array. In: *9th Asia-Pacific Conference on Antennas and Propagation (APCAP)*, Xiamen, China, 04-07 August. IEEE; 2020. pp. 1-2
- [43] Afifi A, Sebak A-R. Wideband 4×4 butler matrix in the printed ridge gap waveguide technology for millimeter-wave applications. *IEEE Transactions on Antennas and Propagation*. 2020;**68**(11):7670-7675
- [44] Yu Y, Jiang ZH, Zhang J-D, Wu W. Broadband millimeter-wave endfire circularly polarized array with a low-profile feeding structure. *IEEE Transactions on Antennas and Propagation*. 2022;**70**(8):7270-7275
- [45] Tan YCM, Guan Hong N. 64-elements mmWave detachable phased array antenna for 5G 26GHz band. In: *2020 IEEE International Symposium*

on Antennas and Propagation and  
North American Radio Science  
Meeting. Montreal, QC, Canada: IEEE;  
2020. pp. 1317-1318

[46] Valkonen R, Doumanis E. Analysis  
and design of mm-Wave phased  
array antennas for 5G access. In: IEEE  
International Symposium on Antennas  
and Propagation and USNC-URSI Radio  
Science Meeting, Atlanta, GA, USA,  
07-12 July 2019. IEEE; 2019. pp. 611-612

[47] Islam MA, Karmakar NC. An 8×8  
mm-wave LP ACMPA array for a long-  
range mm-wave chipless RFID tag-sensor  
reader. *IEEE Journal of Radio Frequency  
Identification*. 2021;5(1):53-63

[48] Verma PK, Kumar R, Singh VK,  
Kumar A. Dual radiator based low profile  
fan beam antenna for millimeter wave  
fencing system. *International Journal  
of Advances in Microwave Technology*.  
2021;6(1):254-259

[49] Lima de Paula I et al. Cost-effective  
high-performance air-filled SIW antenna  
array for the global 5G 26 GHz and 28  
GHz bands. *IEEE Antennas and Wireless  
Propagation Letters*. 2021;20(2):194-198

[50] Khalily M et al. Broadband mm-wave  
microstrip array antenna with improved  
radiation characteristics for different  
5G applications. *IEEE Transactions  
on Antennas and Propagation*.  
2018;66(9):4641-4647

[51] Borhani Kakhki M et al. Millimeter-  
wave beam-tilting vivaldi antenna with  
gain enhancement using multilayer FSS.  
*IEEE Antennas and Wireless Propagation  
Letters*. 2018;17(12):2279-2283

[52] Mantash M, Kesavan A, Denidni TA.  
Beam-tilting endfire antenna using a  
single-layer FSS for 5G communication  
networks. *IEEE Antennas and Wireless  
Propagation Letters*. 2018;17(1):29-33